Chapter-5

A Molecular Theory Including Hard Rod Interactions of Liquid Crystalline Phases Exhibited by Strongly Polar Compounds

5.1 Introduction

As described in chapter-1, liquid crystals composed of highly polar molecules are known to exhibit a variety of unusual phenomena [1] like a first order N-N transition, SmA_1-SmA_d transition, a re-entrant nematic (N_R) lake and an N-N transition associated with the SmA_1-SmA_d transition (see section 1.4, chapter-1 for details). In pervious chapters (chapters-2 and 3), we have developed a molecular theory to describe these phase transitions. The basic concept in the model we adopt [2] is that, as the intermolecular separation (r) is reduced due to cooling or due to increase of pressure, the molecular pairs can change over from the anti-parallel (A) to the parallel (P) configuration (see chapter-2, section 2.2 for details). The medium is treated as an equilibrium *mixture* of the A and P types of pairs. Recent experiments [3, 4] showing the presence of *polar* short range order at low temperatures support this model. The reentrant phases follow as natural consequences of the temperature variation of the relative concentrations of the two species.

Several experimental investigations have been carried out on the phase transition temperatures of such liquid crystals as functions of pressure. In particular, it is seen that the SmA_d phase gets bounded in the p-T plane and the SmA_1- N_R transition temperature increases monotonically with pressure [5, 6] (see figure 5.1). High pressure studies on the binary mixtures of hexyloxy cyanobiphenyl (6OCB) and its higher homologue (8OCB) [7] show that the SmA_d phase is less stable for mixtures with higher concentrations of the shorter homologue (see figure 5.2).

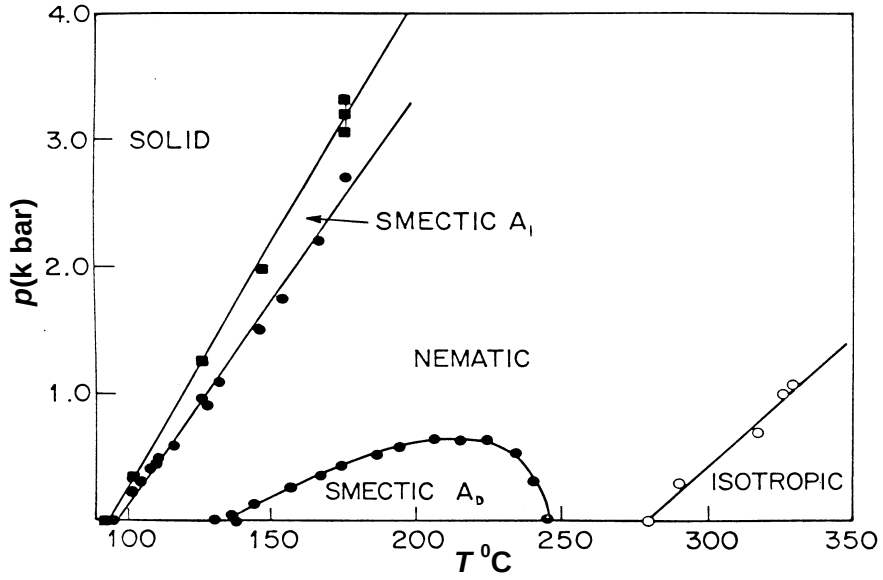

Figure - 5.1. Pressure (*p*) - temperature (*T*) phase diagram [5] of octyloxy benzoyloxycyano-stilbene showing double reentrance at atmospheric pressure. The SmA_d phase gets bounded at higher pressures.

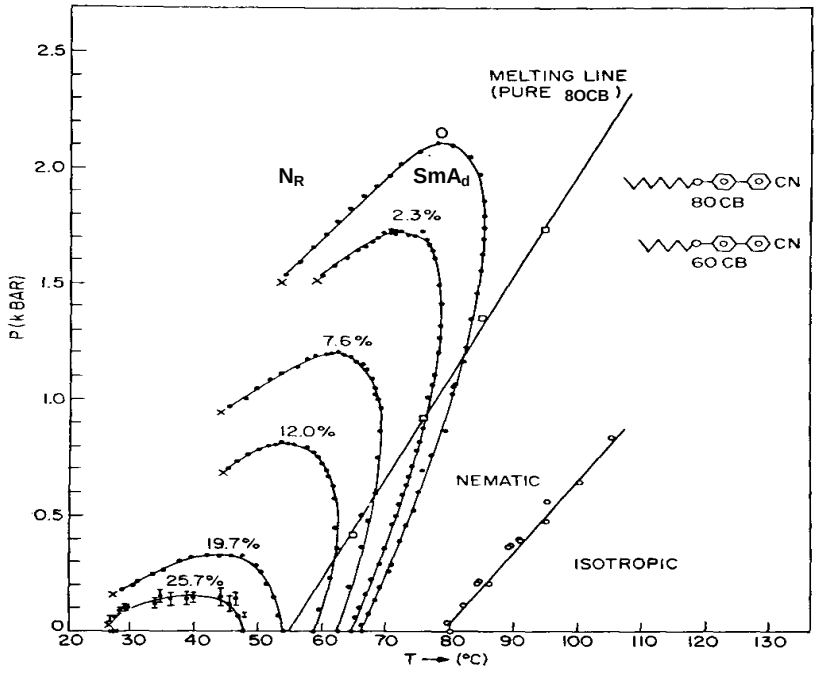

Figure – 5.2. Experimental *p-T* phase diagram [7] of 8OCB-6OCB mixtures. The numbers indicate the concentration of the shorter homologue 6OCB.

To describe *p-T* phase diagrams theoretically, an explicit calculation of pressure is desirable. For this purpose, packing effects which take into account the

hard rod features of molecules have to be considered. Even though many experimental investigations have been carried out on the *p-T* phase diagrams of highly polar compounds, there is no detailed molecular theory to describe them. A thermodynamic theory has been developed by Clark [8]. Indekeu and Berker have developed a spin gas model [9], in which the pressure is simply assumed to be proportional to the inverse of molecular separation. Recently Sear and Jackson [10], have developed a hard rod model of a binary mixture consisting of interconverting monomers and dimers following the method of Koda and Kimura [11]. In this model [10], the temperature comes into picture through the equilibrium constant for the monomer-dimer interconversion and the calculation is restricted to the packing fraction-temperature phase diagrams. In the present chapter, we extend our mean field model of highly polar compounds to include the hard rod features and develop a hybrid model. This allows us to calculate different phase diagrams as functions of pressure.

Several hard rod models of liquid crystals have been developed over the past decades. Onsager [12] was the first to show that packing effects alone can stabilise the nematic phase for long rod like molecules with aspect ratios ~ 100. Molecular shape plays a more definitive role in stabilising the smectic phase compared to the nematic phase. In fact, computer simulation studies [13] show that a system of hard ellipsoids does not form a smectic phase due to packing effects alone. On the other hand, computer simulation studies [13], experiments [14] and a few specific theoretical models [15, 16, 17, 18], show that a system of hard *spherocylinders* can form the nematic and smectic-A phases. As explained by Wen and Meyer [17], the SmA phase is stabilised since the loss of entropy in the formation of layering order is more than compensated by the gain in entropy due to the increased freedom of molecules within the layers. Many authors have extended hard rod models of nematics to develop models of the smectic phase. The scaled particle theory [18], the density functional theory [16, 19], models with both attractive and hard rod features [15, 20] *etc*. have been used for this purpose.

Since in our model of polar compounds, the medium is assumed to be a *mixture* of antiparallel and parallel pairs, we consider hard rod models of binary mixtures [11, 21]. As described in the previous chapters, the relative concentration of

antiparallel and parallel pairs is not a constant, but varies with both temperature and pressure making the calculations quite tedious. Hence, in the present chapter, we adopt the relatively simple theory of hard rod mixtures developed by Koda and Kimura [11] for molecules with perfect orientational order and extend it to develop a hybrid model.

We have shown in chapter-2 (see figure 2.5) that the difference in the configurational energy (ΔE) between A and P types of pairs is a sensitive function of the intermolecular separation and hence the density of the medium. However, as the medium is cooled across the temperatures corresponding to the stability of reentrant phases, the density increases monotonically [5]. Hence, for the sake of simplicity, in our earlier discussions we assumed ΔE to be a function of temperature. In the present chapter, we express ΔE as a function of density *i.e.*, the packing fraction and calculate the pressure explicitly. In the next section, we develop the theoretical model.

5.2 Theoretical model

For the sake of convenience, we have made the following *changes in the notations*:

(i) All the variables connected with parallel (P) and antiparallel (A) types of dimers are indicated by the suffixes '1' and '2' respectively, instead of the suffixes 'A' and 'P'.

(ii) The configurational energy difference is expressed in terms of packing fraction and hence, the interaction parameter is denoted by 'A' instead of R_1.

(iii) The vector representing the smectic density modulation is denoted by $\vec{\boldsymbol{k}}$ instead of $\vec{\boldsymbol{q}}$ and q is used to denote the length ratio of A and P types of pairs, adopting the notation used by Koda and Kimura [11]

(iv) The parameter a is used to represent the normalised amplitude of the smectic density modulation and is equivalent to τ used earlier.

(v) The normalised distribution functions are denoted by ϕ instead of f.

5.2.1 Assumptions

As in the earlier chapters, we assume the medium to be a binary mixture of parallel (P) and antiparallel (A) types of dimers. The configurational energy difference is written in terms of packing fraction as

$$\Delta E = E_2 - E_1 = A\, k_B T^* \left(\frac{\eta}{\eta^*} - 1 \right) \tag{5.1}$$

where, A is a dimensionless interaction parameter, k_B the Boltzmann constant, T^* some reference temperature, η the packing fraction, η^* the packing fraction at which $E_2 = E_1$. For $\eta > \eta^*$, ΔE is positive which means that E_1 is more negative than E_2 and the P-type configuration is favoured over the A-type configuration.

Both A and P types of dimers are assumed to be right circular cylinders of the *same volume* v, but of different lengths l_2 and l_1 respectively ($l_2 > l_1$) and the corresponding diameters are denoted by D_2 and D_1. We define

$$q = \frac{l_2}{l_1} = \frac{D_1^2}{D_2^2} . \tag{5.2}$$

The average packing fraction is given by,

$$\eta = \frac{N_1 v + N_2 v}{V} = \frac{N v}{V} \tag{5.3}$$

where N_1 and N_2 are the number of P and A types of pairs respectively, V is the system volume, $v = \frac{\pi D_1^2 l_1}{4} = \frac{\pi D_2^2 l_2}{4}$ and $N = N_1 + N_2$ is the total number of pairs. The volume fractions which are the same as the relative fractions of P and A types of pairs respectively are

$$X_1 = \frac{N_1}{N} \quad , X_2 = \frac{N_2}{N} \tag{5.4}$$

so that $X_1 + X_2 = 1$.

For simplicity especially in the calculation of excluded volume effects, the cylinders are assumed to have perfect orientational order and aligned along the Z-axis. As most of the phenomena like reentrance occur well below the nematic - isotropic transition temperature, this assumption is reasonable.

5.2.2 Free energy

5.2.2.1 Hard rod component

The hard rod part of the Helmholtz free energy (F^{h}) is calculated in the second virial approximation following Koda and Kimura [11]. Let $P_\nu(\boldsymbol{r})$ be the packing fraction of cylinders of length l_ν at the position $\boldsymbol{r}=(x,y,z)$. Obviously, the fractional volume occupied by the species of the type ν (= 1 or 2) is $\int_V d\boldsymbol{r}\, P_\nu(\boldsymbol{r}) = N_\nu\, v$.

F^{h} can be expressed as a functional of $P_\nu(\boldsymbol{r})$ in the form [11]

$$\frac{F^{h}}{k_B T} = \sum_\nu N_\nu \Lambda_\nu(T) + \sum_\nu \frac{1}{v}\int_V d\boldsymbol{r}\, P_\nu(\boldsymbol{r}) \ln P_\nu(\boldsymbol{r})$$

$$-\frac{1}{2}\sum_\nu \sum_{\nu'} \frac{1}{v^2}\int_V d\boldsymbol{r_1}\, d\boldsymbol{r_2}\, P_\nu(\boldsymbol{r}_1)\, P_{\nu'}(\boldsymbol{r}_2)\, b_{\nu\nu'}(\boldsymbol{r}_1,\boldsymbol{r}_2)$$

$$+ \{ \text{Higher order terms in } P_\nu(\boldsymbol{r}) \} \qquad (5.5)$$

where T is the temperature and $\Lambda_\nu(T)$ which is a function of only T is the contribution from kinetic energy. Since we carryout the calculations as a function of η at a fixed temperature, $\Lambda_\nu(T)$ is not relevant in determining η corresponding to the phase transition. The second term is the contribution from the entropy of mixing and the third term is due to the hard core interactions which are restricted to second virial term, and $b_{\nu\nu'}(\boldsymbol{r}_I,\boldsymbol{r}_j)$ is the Mayer function. The latter is defined as

$$b_{\nu\,\nu'}(\boldsymbol{r}_i\,,\boldsymbol{r}_j\,) = \exp(-U_{ij}/k_{\mathrm{B}}T) - 1 \tag{5.5a}$$

where U_{ij} is the two particle interaction potential. For *hard* spheres of diameter D, with r_{ij} denoting the interparticle distance, this can be written as

$$r_{ij} \geq D, \qquad U_{ij} = 0, \quad b_{\nu\,\nu'}(\boldsymbol{r}_i\,,\boldsymbol{r}_j\,) = 0.$$

$$r_{ij} < D, \qquad U_{ij} = \infty\,, \quad b_{\nu\,\nu'}(\boldsymbol{r}_i\,,\boldsymbol{r}_j\,) = -1 \tag{5.5b}$$

In the present calculations involving *parallel* hard cylinders, the Mayer function is given by [11]

$$b_{\nu\,\nu'}\,(\boldsymbol{r}_i\,,\boldsymbol{r}_j\,) = -H\left[\left(\frac{l_\nu + l_{\nu'}}{2}\right)^2 - (z_i - z_j)^2\right] H\left[\left(\frac{D_\nu + D_{\nu'}}{2}\right)^2 - (x_i - x_j)^2 - (y_i - y_j)^2\right] \tag{5.6}$$

where $H(\gamma) = 0$ for $\gamma \leq 0$ (*i.e.*, when the rods are not in contact) and $H(\gamma) = -1$ for $\gamma > 0$ (*i.e.*, when the rods interpenetrate) and the Z - axis is taken along the director.

The packing fraction of each kind of cylinder is uniform in the *nematic* phase and is given by

$$P_\nu\,(\boldsymbol{r}) = \frac{N_\nu v}{V} \tag{5.7}$$

while that in the SmA phase is a periodic function of z, *i.e.*, [11]

$$P_\nu\,(\boldsymbol{r}) = \frac{N_\nu\, v}{V}\,\rho_\nu\,(z). \tag{5.8}$$

We define $\zeta = z/l_1$ *i.e.*, take l_1 as unit of length. Substituting equations (5.6) and (5.8) in equation(5.5) and restricting to terms quadratic in ρ, we can write the free energy per pair

$$f^{\,\mathrm{h}} = \frac{F^{\,\mathrm{h}}}{N\,k_{\mathrm{B}}\,T} \tag{5.9}$$

as a functional of $\rho_v(\zeta)$ as:

$$f^{h}[\rho_1(\zeta), \rho_2(\zeta)] = X_1\left[\Lambda_1(T) + \ln\frac{N_1 v}{V}\right] + X_2\left[\Lambda_2(T) + \ln\frac{N_2 v}{V}\right]$$

$$+ \frac{X_1}{L}\int_L d\zeta\, \rho_1(\zeta)\ln\rho_1(\zeta) + \frac{X_2}{L}\int_L d\zeta\, \rho_2(\zeta)\ln\rho_2(\zeta)$$

$$+ 2X_1^2\,\eta\,\frac{1}{L}\int_L d\zeta\, d\zeta'\, \rho_1(\zeta)\,\rho_1(\zeta')\,H\left[1-(\zeta-\zeta')^2\right]$$

$$+ 2X_2^2\,\eta\,\frac{1}{qL}\int_L d\zeta\, d\zeta'\, \rho_2(\zeta)\,\rho_2(\zeta')\,H\left[q^2-(\zeta-\zeta')^2\right]$$

$$+ X_1 X_2\,\eta\left(1+\frac{1}{\sqrt{q}}\right)^2\frac{1}{L}\int_L d\zeta\, d\zeta'\, \rho_1(\zeta)\,\rho_2(\zeta')\,H\left[\left(1+\frac{q}{2}\right)^2-(\zeta-\zeta')^2\right] \quad (5.10)$$

where L is the system size along Z- axis in units of l_1.

The sinusoidal perturbation of $\rho_v(\zeta)$ in smectic A can be written as

$$\rho_v(\zeta) = 1 + a_v \cos k\zeta \quad (5.11)$$

where $k = \frac{2\pi}{d}$ is the (dimensionless) wave number of the perturbations with d as the average layer spacing in units of l_1, and a_v represent amplitudes equivalent to order parameters in smectic A. Substituting equation(5.11) into equation(5.10) and restricting to terms quadratic in a_1 and a_2, we can write,

$$f^{\,h} = \frac{F^{\,h}}{N\,k_B\,T} = f_N + \delta f_S^{\,h}. \qquad (5.12)$$

where, the nematic free energy per pair (f_N) arises from the hard rod interactions and the pairing energy (ΔE) since the medium is assumed to have perfect orientational order. We have, with $a = 0$,

$$\frac{F_N}{Nk_BT} = f_N = X_1\left[\Lambda_1(T) + \ln\frac{N_1 v}{V}\right] + X_2\left[\Lambda_2(T) + \ln\frac{N_2 v}{V}\right] + \eta\,[4 + X_1X_2 b(q)] + X_2\,\frac{\Delta E}{k_BT} \qquad (5.13)$$

$$\text{where} \quad b(q) = \frac{v_{ex}}{v} - 8 \qquad (5.13a)$$

and v_{ex} is the excluded volume given by

$$v_{ex} = \frac{\pi}{4}(D_1 + D_2)^2\,(l_1 + l_2) = v\left[\left(1 + \frac{1}{\sqrt{q}} + \sqrt{q}\right)^2 - 1\right]. \qquad (5.13b)$$

The smectic perturbation energy is,

$$\frac{\delta F_S^{\,h}}{N\,k_B\,T} = \delta f_S^{\,h} = X_1\,\frac{a_1^{\,2}}{4} + X_2\,\frac{a_2^{\,2}}{4} + 2\,X_1^{\,2}\,\eta\,a_1^{\,2}\,\frac{\sin k}{k} + 2\,X_2^{\,2}\,\eta\,a_2^{\,2}\,\frac{\sin qk}{qk}$$

$$+\; X_1\,X_2\,\eta\left(1 + \frac{1}{\sqrt{q}}\right)^2\,\frac{a_1\,a_2}{k}\sin\left[\frac{k(1+q)}{2}\right] \qquad (5.14)$$

5.2.2.2 Attractive component

The attractive component of the energy of i^{th} pair in the smectic medium is given by,

$$U_{iv} = -\,U_o\,\eta\,\sum_{v'}\,\alpha_{vv'}\,X_{v'}\,a_{v'}\cos(k\zeta_{iv}) \qquad (5.15)$$

where U_o is an interaction parameter. $\alpha_{vv'}$ are the McMillan parameters defined as

$$\alpha_{vv} = 2\,\exp[-(\pi\,r_0/d_{vv})^2] \qquad (5.16)$$

and the mutual interaction parameter, assuming the geometric mean (GM) rule is

$$\alpha_{\nu\nu'} = \sqrt{\alpha_{\nu\nu}\ \alpha_{\nu'\nu'}} \tag{5.17}$$

where $d_{11} = r_o + c$ and $d_{22} = r_o + 2c$, with r_o and c being the lengths of aromatic and chain moieties respectively. α_{22} is obviously related to α_{11}.

The total internal energy of N pairs is,

$$U = \frac{N}{2} \sum_{\nu} \langle U_{i\nu} \rangle X_\nu = -\frac{N}{2} U_o \eta \sum_{\nu} \sum_{\nu'} \alpha_{\nu\nu'} X_\nu X_{\nu'} a_\nu a_{\nu'} \tag{5.18}$$

where $\langle\ \rangle$ indicates a statistical average and we have used

$$a_\nu = \langle \cos(2\pi\zeta_{i\nu}/d) \rangle = \int_0^1 d\xi_\nu\ \phi_\nu \cos(\pi\xi_\nu) \tag{5.19}$$

with $\xi_\nu = \frac{2\zeta_\nu}{d} = \frac{k\zeta_\nu}{\pi}$ as the reduced coordinate and ϕ_ν is the normalised distribution function for the ν-type of pairs.

The entropy of N pairs is,

$$\mathcal{S} = -N k_B \sum_{\nu} X_\nu \int_0^1 d\xi_\nu\ \phi_\nu \ln\phi_\nu \tag{5.20}$$

The attractive part of the *smectic* free energy in the mean field approximation for the medium with perfect orientational order is given by, $\Delta F_S^a = U - T\mathcal{S}$,

$$i.e., \qquad \delta f_S^a = \frac{\Delta F_S^a}{N k_B T} = -\frac{U_o \eta}{2 k_B T} \sum_{\nu} \sum_{\nu'} \alpha_{\nu\nu'} X_\nu X_{\nu'} a_\nu a_\nu + \sum_{\nu} X_\nu \int_0^1 d\xi_\nu\ \phi_\nu \tag{5.21}$$

5.2.2.3 Total free energy due to smectic ordering

The total free energy due to smectic ordering is given by,

$$\delta f_S = \delta f_S^{\,h} + \delta f_S^{\,a} = -X_1 X_2 a_1 a_2 \tilde{C} + \sum_\nu \left(-\frac{X_\nu a_\nu^{\,2} C_\nu}{2} + X_\nu \int_0^1 d\xi_\nu \ \phi_\nu \ln \phi_\nu \right) \quad (5.22)$$

where we have defined,

$$C_1 = \left[\frac{U_o}{k_B T} \alpha_{11} - 4\, j_o(k) \right] \eta X_1 - \frac{1}{2} \quad (5.23)$$

$$C_2 = \left[\frac{U_o}{k_B T} \alpha_{22} - 4\, j_o(qk) \right] \eta X_2 - \frac{1}{2} \quad (5.24)$$

$$\tilde{C} = C_{12} = C_{21} = \left\{ \frac{U_o}{k_B T} \alpha_{12} - \frac{1}{k} \left(1 + \frac{1}{\sqrt{q}} \right)^2 \sin\left[\frac{k(1+q)}{2} \right] \right\} \quad (5.25)$$

where $j_o(m) = \dfrac{\sin(m)}{m}$ is the zeroth order Bessel function.

The distribution function ϕ_ν for ν^{th} species obtained by minimising δf_S is:

$$\phi_\nu = \frac{1}{Z_\nu} \exp[(\, a_\nu C_\nu + X_{\nu'}\, a_{\nu'}\, \eta \tilde{C}) \cos \pi \xi_\nu] \quad (5.26)$$

where ν' now represents the second species, and Z_ν are the appropriate normalising integrals.

Substituting ϕ_ν in equation(5.22), we get,

$$\delta f_S = \sum_\nu \left(\frac{X_\nu a_\nu^{\,2} C_\nu}{2} - X_\nu \ln Z_\nu \right) + X_1 X_2 a_1 a_2 \tilde{C} \quad (5.27)$$

Expanding $\ln Z_\nu$ and restricting to terms quadratic in a_1 and a_2, which is valid close to the SmA-N transition, we get,

$$\delta f_S = \frac{X_1 a_1^2}{4}(2C_1 - C_1^2 - X_1 X_2 \tilde{C}^2) + \frac{X_2 a_2^2}{4}(2C_2 - C_2^2 - X_1 X_2 \tilde{C}^2)$$

$$+ X_1 X_2 a_1 a_2 \tilde{C}\left(1 - \frac{C_1 + C_2}{2}\right). \quad (5.28)$$

This can be written as,

$$\delta f_S = \begin{bmatrix} a_1 & a_2 \end{bmatrix} \begin{bmatrix} S_{11} & S_{12} \\ S_{21} & S_{22} \end{bmatrix} \begin{bmatrix} a_1 \\ a_2 \end{bmatrix} \quad (5.29)$$

where,

$$S_{11} = \frac{X_1}{4}(2C_1 - C_1^2 - X_1 X_2 \tilde{C}^2)$$

$$S_{22} = \frac{X_2}{4}(2C_2 - C_2^2 - X_1 X_2 \tilde{C}^2)$$

$$S_{12} = S_{21} = \frac{1}{2} X_1 X_2 \tilde{C}\left(1 - \frac{C_1 + C_2}{2}\right). \quad (5.30)$$

$\delta f_S = 0$ determines the N-SmA transition point. This condition is equivalent to

$$\det(S) = S_{11} S_{22} - S_{12} S_{21} = 0. \quad (5.31)$$

Using equations(5.30) at the transition point, we get,

$$X_1 X_2 \tilde{C}^2 - C_1 C_2 = \Delta = 0 \quad (5.32)$$

5.2.3 Expressions for k and X_2

k can be found by minimising δf_S given by equation(5.29). The value k_c at the transition is given by,

$$k_c = \frac{X_1 X_2 \tilde{C}\left(1+\frac{1}{\sqrt{q}}\right)^2 \sin\left[\frac{k_c(1+q)}{2}\right] - 2C_1 X_2 \frac{\sin(qk_c)}{q} - 2C_2 X_1 \sin k_c}{X_2 \tilde{C}\left(1+\frac{1}{\sqrt{q}}\right)^2 \left(\frac{1+q}{2}\right) \cos\left[\frac{k_c(1+q)}{2}\right] - 2C_1 X_2 \cos(qk_c) - 2C_2 X_1 \cos k_c} \quad (5.33)$$

In view of the assumption of saturated nematic order, the N - SmA transition is second order in nature and at the transition point $X_2 = X_2^N$. Therefore X_2 is found by the condition $\frac{\partial F_N}{\partial X_2} = 0$. This gives,

$$X_2 = \frac{1}{1 + \exp\left[\eta(1-2X_2)\, b(q) + \frac{\Delta E}{k_B T}\right]} \quad (5.34)$$

5.2.4 Expression for pressure

We have $p = -\left(\frac{\partial F}{\partial V}\right)_T$. As above, at the N - SmA transition point, $p = p_N$. Hence,

$$\frac{pv}{k_B T} = -\left[\frac{\partial (F_N v / k_B T)}{\partial V}\right]_T$$

Using equation (5.13) we get,

$$\frac{pv}{k_B T} = \eta + \eta^2 \left[4 + \frac{X_2 A}{T_R \eta^*} + X_1 X_2 b(q)\right] \quad (5.35)$$

We can consider a molecule of a typical mesogenic compound as a cylindrical rod of length ≈20Å and diameter ≈5Å. Hence, $v \approx 400 Å^3$. This gives, $pv/(k_B T) = 1$ for $p \approx 0.5$ kbar at T=350K.

5.2.5 Expression for Gibbs free energy

We have, at the transition point the Gibbs free energy, $G = G_N = F_N + pV$. Therefore,

$$\frac{G_N}{N k_B T} = 1 + X_1\left[\Lambda(T) + \ln\left(\frac{N_1 v}{V}\right)\right] + X_2\left[\Lambda(T) + \ln\left(\frac{N_2 v}{V}\right)\right]$$

$$+ \eta\left\{\frac{X_2 A}{T_R \eta^*} + 2[4 + X_1 X_2 b(q)]\right\} + \frac{X_2 \Delta E}{k_B T} \qquad (5.36)$$

5.2.6 Method of calculation

The parameters of our model are A, η^*, q, U_o (see equations 5.1, 5.2 and 5.15) and α (see equation 5.16). U_o is an interaction parameter taken to be = 4.541 $k_B T^*$ with T^*=500K. This corresponds to the MS potential used in the previous chapters. The parameter A which determines the steepness of variation of ΔE with respect to η and is equivalent to R_1 used in the previous chapters. We have shown in chapter-3 (section 3.3.1.1) that R_1 varies as the fourth power of the McMillan parameter α_2. In the present calculations we use very low values of α_2. Hence we use low values of A. Fixing η and T_R, the values of k and X_2 are found by self consistency of equations 5.33 and 5.34. With these values, Δ (see equation 5.32) is calculated for η varying from 0 to η_{max} (about 0.9 for hexagonal close packing of cylinders). Δ>0 corresponds to the smectic phase. The values of η corresponding to the N-SmA transition are located by the condition Δ=0. If X_1 is large, the smectic has monolayer order (*i.e.*, SmA_1), otherwise it is SmA_d. Similarly, we denote the nematic with a larger (smaller) value of X_1 as the N_1 (N_d) phase. As in the previous chapters, the suffix 'R' in N_R, N_{R1} and N_{Rd} denotes a reentrant nematic phase. In the next section, we present the results.

5.3 Results and discussions

Even though we have assumed a saturated orientational order, there can be a first order N-N transition involving a jump in X_1. At this transition, the Gibbs free energies corresponding to the two phases having (η, X_1) and (η', X_1') at a particular pressure become equal. We first discuss the nematic to nematic transition.

5.3.1 Nematic - nematic transition

It can be recalled that q is the length ratio of the A and P types of pairs (see equation 5.2), A is the interaction parameter for the difference in the configurational energies between the pairs (see equation 5.1) and for the packing fraction $\eta > \eta^*$, P-type of pairs are favoured over the A-type of pairs. We have calculated the variation of pressure with packing fraction for A = 3, η^* = 0.55, q = 1.2 and T_R = 0.4 (figure 5.3a).

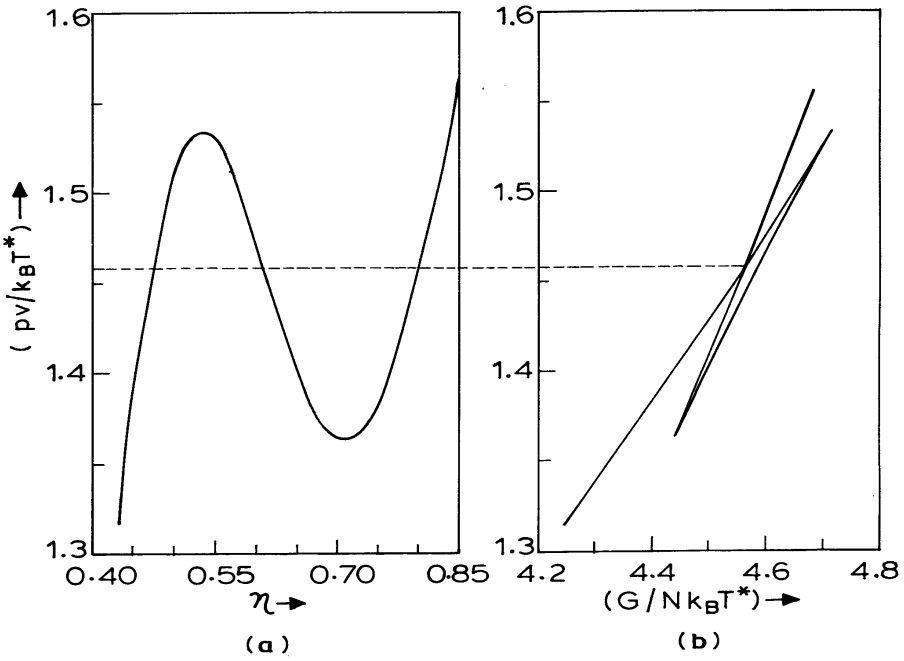

Figure - 5.3. (a) Variation of pressure with packing fraction and (b)variation of pressure with Gibbs free energy, for A = 3, η^* =0.55, q=1.2 and T_R = 0.4. The dashed line shows the pressure at which the Gibbs free energies of the two phases become equal indicating a nematic to nematic phase transition.

An N_1-N_d transition occurs at a value of pressure indicated by the dashed line, at which the Gibbs free energies of the two phases become equal (figure 5.3b).With the same values of η^* and q, the N_1-N_d transition lines are shown in the p-T plane in figure 5.4, for different values of A. The transition is from the N_1 phase (above the line) to the N_d phase (below the line). The N_1-N_d transition temperature increases with pressure and the first order N_1-N_d transition line ends in a critical point. The critical

point shifts to higher values of (p,T) on increasing A. Thus, the possibility of observing such a transition increases for larger values of A. Since A is proportional to ΔE (see equation 5.1), the value of A can be expected to increase with the dipole moment of the molecules. Indeed, while 7CB (heptyl cyanobiphenyl) does not exhibit the N-N transition, the analogous molecule with an ester group dipole adding to that of the cyano group (cyanophenyl heptylbenzoate or CP7B) exhibits the transition [22] (see figure 2.2, chapter-2). It can be seen from figure 5.4 that the transition temperature has an approximately linear dependence on pressure as seen experimentally [23]. However, the theoretical slope (≈ 4 bar/K with T_{NI} ≈350K, see discussion under equation 5.35) is much less than the experimental value (≈60 bar/K, [23]). Thus, the pressure values are underestimated in our theory. The reason for this discrepancy is that the hard core interactions are *limited* to the second virial term and such an approximation is known to underestimate the pressure even for the N- I transition [24]

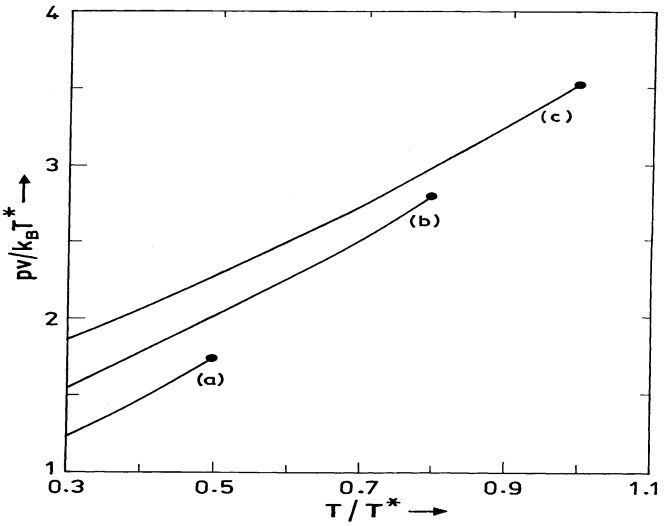

Figure - 5.4. The p-T phase diagram for $\eta^* = 0.55$, $q = 1.2$, showing the N-N transition lines for different values of A;(a) $A = 3$, (b) $A = 5$ and (c) $A = 6.5$. The transition is from the N_1 phase (above the line) to the N_d phase (below the line). The first order N_1 -N_d transition line ends in a critical point indicated by a filled circle.

The above calculations have been made with a fixed length ratio q between the two types of pairs. q increases with chain length. Also the value of A, which determines the slope of ΔE with respect to η, increases with chain length in a homologous series as explained in chapter-3 (section 3.3.1.1). Near q = 1.5, if the

chain length is increased by 50%, ΔE increases by an order of magnitude (see chapter-3, section 3.3.1.1), whereas q increases only by about 10%. To study the effect of q independently, we have calculated the diagram shown in figure 5.5a with A = 5, η^*=0.55 and T_R fixed at 0.85.

As q is decreased, the N_1-N_d transition occurs at a higher pressure (figure 5.5a) with a smaller jump in X_2 and there is no N_1-N_d transition for q less than the critical value ≈1.44 for A=5 (figure 5.5b). However, the variation in the transition pressure is relatively weak as a function of q, compared to that with A (see figure 5.4).

At the N_d- N_1 transition, the downward jump in X_2 is accompanied by a jump in η to higher values (figure 5.3a), resulting in a better packing at the same p and T values and this packing effect obviously depends on q. Hence, in general, as the chain length is increased, if the smectic phase does not intervene, the first order nature of the N_1-N_d transition can be expected to become stronger (see figure 5.5) and to occur at a lower temperature at any given pressure (see figure 5.4) due to higher values of both q and A.

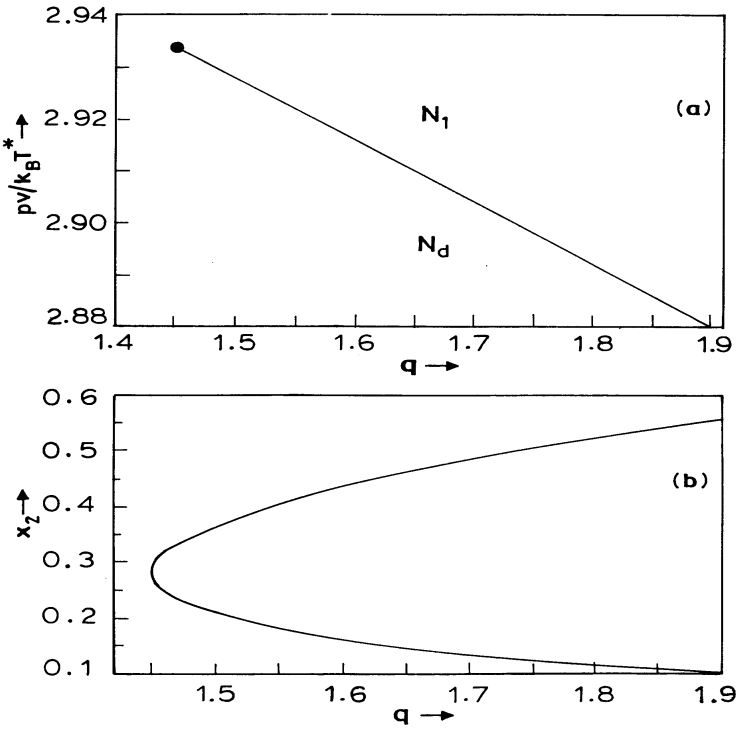

Figure – 5.5. (a) Variation of N_1-N_d transition pressure with q and (b)corresponding variation in X_2 which is double valued, for A=5, η*=0.55 and T_R = 0.85. The filled circle in (a) indicates the N_1-N_d critical point.

5.3.1.1 Significance of negative deviation from the GM rule

We have shown in chapter-2 (see section 2.4.3.2), that in the *absence* of hard rod interactions, a *negative* deviation from the geometric mean (GM) rule in the attractive interaction between the A and P types of pairs is *necessary* to get an N_1-N_d transition and the first order nature of the transition becomes stronger if the deviation is larger. As discussed above, in the present calculations the hard rod effects alone are sufficient to give rise to the N_1-N_d transition even when the nematic order is saturated and the mutual attractive interaction has not been taken into account. Further, an increase of the chain length (*i.e.*, q and A) has the same effect as that of a stronger negative deviation. Obviously, an increase of q makes the A and P types of pairs structurally more dissimilar. This results in a larger excluded volume (given by equation 5.13b). If the two species are geometrically equivalent *i.e*, .if q = 1, v_{ex} = 8 v and from equation (5.13a), $b(q)$ = 0. Otherwise, $b(q)$>0 which would, from equation 5.13, *increase* the free energy of the medium. In theories which consider only the

mean field attractive part, an increase in the free energy requires a negative deviation from GM rule.

Indeed, experiments show that, even the N-I transition temperatures of binary mixtures of nematogens have a negative deviation from the linear dependence on the relative concentration. This has been attributed to a negative deviation from the GM rule in a theory considering only the attractive interactions [25], and later numerically shown to be equivalent to including hard rod interactions between the molecules [26]. Our present argument also clearly shows that the physical origin of a negative deviation from GM rule is related to the excluded volume between the cylinders of different aspect ratios, even when both of them have the *same volume*.

5.3.2 Phase diagrams involving smectics

5.3.2.1 Double reentrance

As we mentioned earlier, the packing effect alone can stabilise the smectic phase[17, 11]. Further, relatively small values of the McMillan parameter α are sufficient to stabilise the smectic phase over *wide ranges* of pressures and temperatures. In our model, as described in chapter-3, where hard rod effects are not considered, the cause of nematic reentrance when the *temperature* is decreased in the SmA_d phase is the rapid change over of the A-type of pairs to P-type, at a temperature *not* low enough to stabilise the SmA_1 phase. In the present calculations, this change over takes place as a function of packing fraction η. When the medium consists of molecules having different lengths, it is difficult to arrange them in layers. In the *absence* of attractive interactions, only this difficulty in packing can destabilise the SmA_d phase. This effect depends on the value of q and is maximum when the medium consists of equal number of A and P types of pairs, *i.e.*, when $X_2 \approx 0.5$. However, since we use small values of q (< 2), though X_2 decreases rapidly when η is increased, the SmA_d phase is not destabilised even when $X_2 \approx 0.5$. Hence, we could not get a *reentrant* sequence for any combination of ΔE and q, by completely ignoring the attractive part of the smectic interactions. Once we include $\alpha_2 \neq 0$, the temperature becomes relevant. At higher temperatures, higher pressures are required to get the N-

SmA transition. When the value of α_2 is small, the A-type to P-type change over does not have a significant influence on the stability of the SmA phase. As α_2 is increased to 0.04, the influence of the A-type to P-type change over can be seen as a clear change of slope in the N-SmA transition line in the *p-T* phase diagram (figure 5.6). The variation of X_2 is smooth and there is a continuous change over between SmA_d and SmA_1 phases.

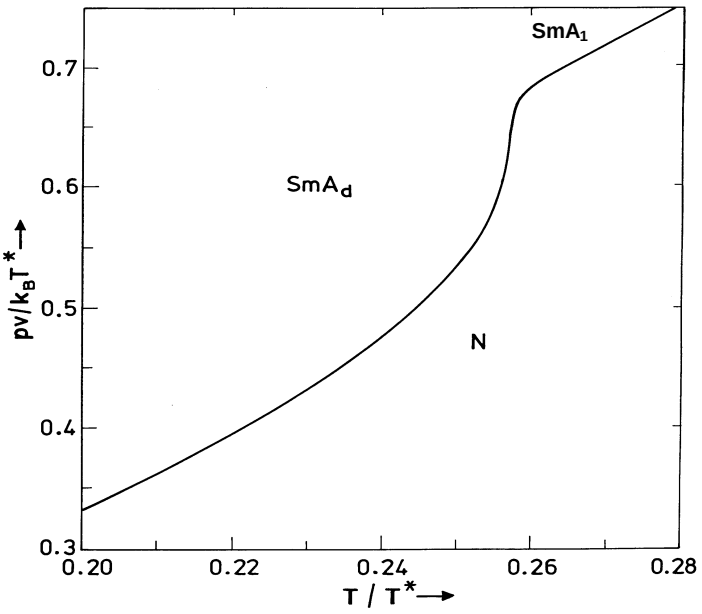

Figure - 5.6. The *p -T* phase diagram obtained for *A* = 1.1, η^* = 0.5, *q* =1.8 and α_2 = 0.04. Note the sudden change in the slope of the phase transition line.

When α_2 is further increased to 0.05, the SmA_d phase is stable at *higher* temperatures also. As the pressure and hence η is increased, X_1 becomes large at a pressure not high enough to stabilise the SmA_1 phase and the nematic phase reenters. At still higher pressures, the SmA_1 phase is stabilised leading to double reentrance as a function of pressure (figure 5.7). At higher temperatures, the SmA_d region gets bounded. If *A* and α_2 are increased to 1.5 and 0.062 respectively, the upward tilt of the closed SmA_d boundary becomes pronounced (figure 5.8). The inset shows the reentrant part of the phase diagram with a magnified scale of the pressure axis.

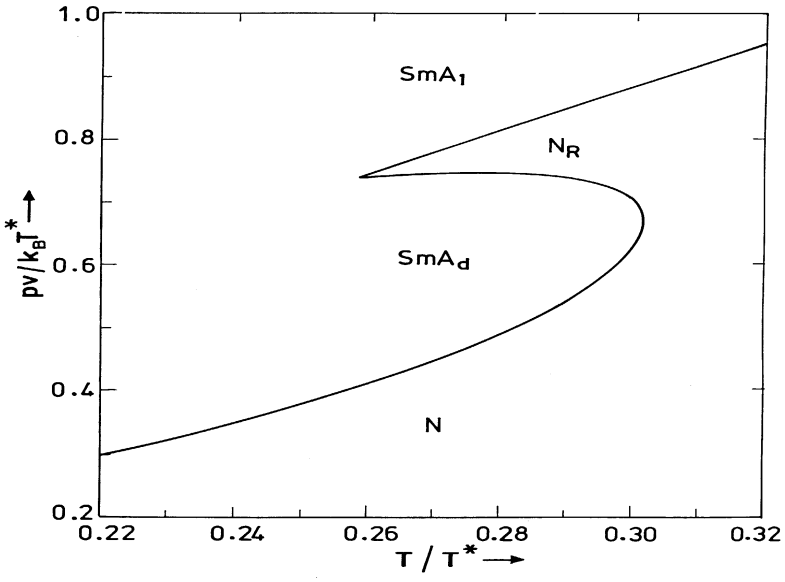

Figure – 5.7. The *p-T* phase diagram showing double reentrance, obtained for A = 1.1, η^* = 0.5, q = 1.8 and α_2 = 0.05.

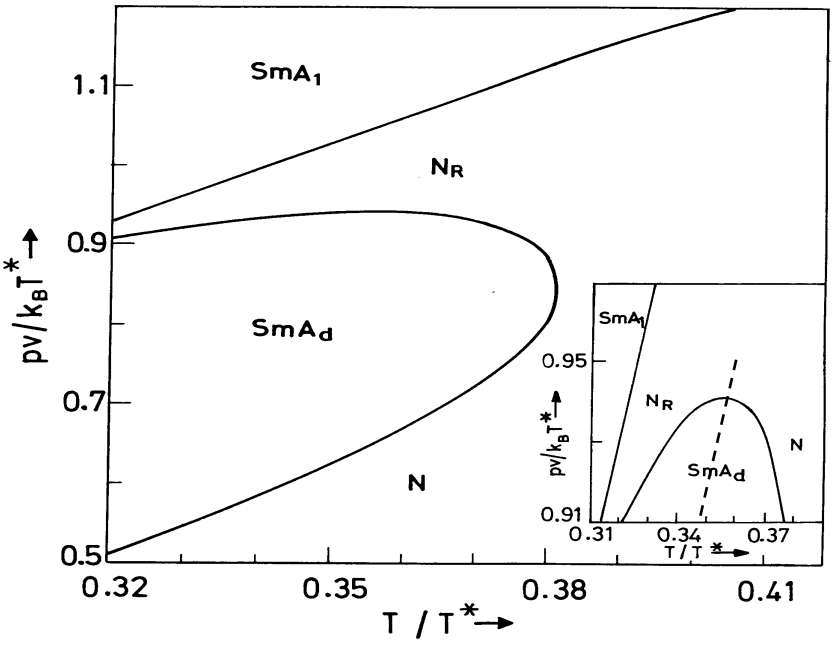

Figure – 5.8. The *p -T* phase diagram obtained for A =1.5, η^* =0.5, q =1.8 and α_2 = 0.062. The inset shows the reentrant part of the phase diagram with a magnified scale of the pressure axis. The axis of the parabolic SmA_d boundary (the dashed line) and the SmA_1-N_R line are roughly parallel.

The theoretical diagram in the inset of figure 5.8 resembles the experimental one (see figure 5.1) [5] on a compound exhibiting a double reentrant sequence. The axis of the parabolic SmA_d boundary and the SmA_1 - N_R line are roughly parallel as in

the experimental curve. However, for the SmA_1 - N_R line, the theoretical slope (≈3 bar/K) is much less than the experimental value (≈30 bar/K, see figure 5.1). The theory underestimates the pressure values due to the second virial approximation as in the N_1-N_d transition (see section 5.3.1).

The *p-T* phase diagrams obtained for $A = 1.5$, $\eta^* = 0.5$, $q = 1.8$ and α_2 varying from 0.048 to 0.066 are shown in figure 5.9.

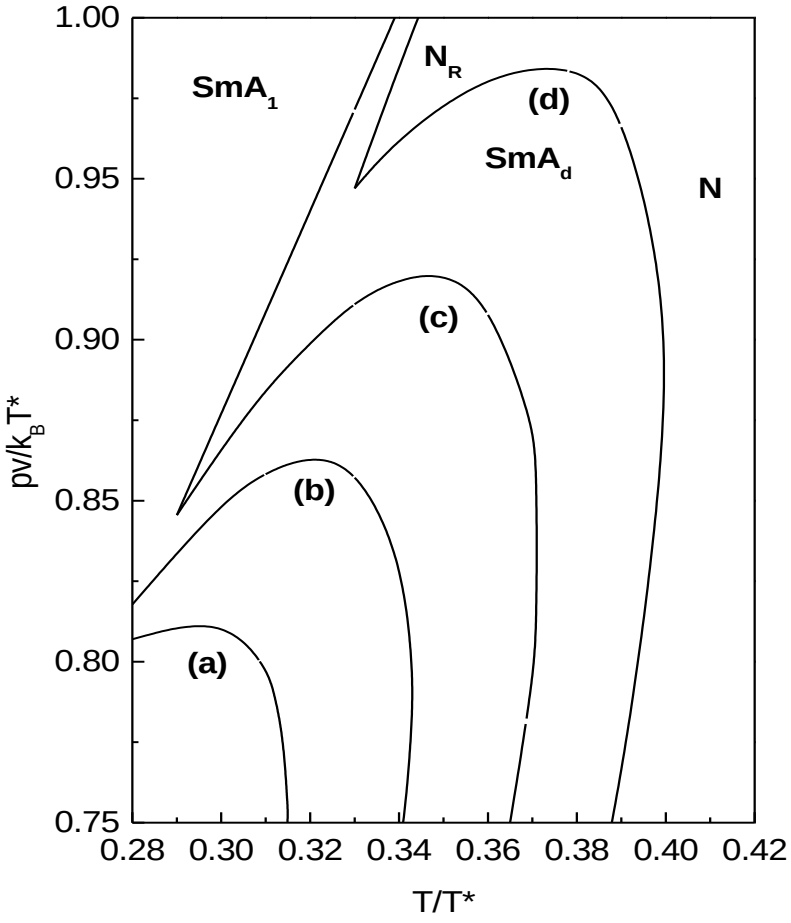

Figure – 5.9. The *p-T* phase diagram obtained for A =1.5, η^* =0.5, q =1.8 for different values of α_2. (a) α_2 =0.048, (b) α_2 =0.054, (c) α_2 =0.06 and (d)α_2 = 0.066. For (a) and (b), the SmA_1-N_R line is not shown.

The SmA_d phase gets bounded in the *p-T* plane and its stability increases as α_2 is increased. For still higher values of α_2, the SmA_d phase continuously changes over to SmA_1 phase without the intervening N_R phase. The theoretical trends are very similar to the experimental ones on mixtures of 6OCB and 8OCB studied by Cladis *et.al.*[5] (see figure 5.2). Since 8OCB has the longer chain length, higher values of α_2

correspond to larger concentrations of 8OCB. We can compare the experimental curve for pure 8OCB with the theoretical curve corresponding to the maximum value of α_2 which can result in the reentrant sequence. We see that, for pure 8OCB, $T_{NI} \approx 350$K and the SmA_d region gets bounded at a pressure ~ 2 k bar. In the theoretical diagram, the SmA_d region gets bounded at $pv/(k_BT^*) \approx 1$. This corresponds to ~0.5k bar (see discussion under equation 5.35). The theory under estimates the pressure values due to the second virial approximation as mentioned earlier.

5.3.2.2 Double reentrance with N_1-N_d transition

As we discussed in the previous chapters, the N_1-N_d transition can occur in association with the SmA_1-SmA_d transition in the reentrant part of the phase diagram. As we have discussed in chapter-3 (see section 3.4.2.2), our model predicts such a phase sequence even in the absence of hard core interactions, over a very small range of the model parameters (see figure 3.21). In the present calculations, in which the hard rod interactions are included, again we find a similar trend over a very small range of the model parameters. The *p-T* phase diagram obtained when *A* is increased to 1.52 with $\eta^* = 0.5$, $q = 1.8$ and $\alpha_2 = 0.042$ is shown in figure 5.10. As mentioned earlier, $\Delta > 0$ (see equation 5.32) corresponds to the SmA phase. Since we have restricted the free energy expansion to the quadratic powers in the order parameters, the equations are valid only close to the N-SmA transition. Hence, we can not locate the SmA_1-SmA_d transition if it occurs well within the SmA phase. However, for $\Delta > 0$, at some values of (*p,T*) the free energies become equal for two different values of X_2. This is indicative of a SmA_1-SmA_d transition near those values of (*p,T*). Such values are shown with a dashed line in figure 5.10. As in figure 5.4, the N_1-N_d transition ends in a critical point at higher values of *p* and *T*.

We get a similar phase diagram even if we assume the McMillan parameter of the P-type of pairs (α_1) to be zero. This is shown in figure 5.11 for A=1.52, $\eta^* = 0.5$, q=1.8, $\alpha_2 = 0.05$ and α_1 assumed to be zero.

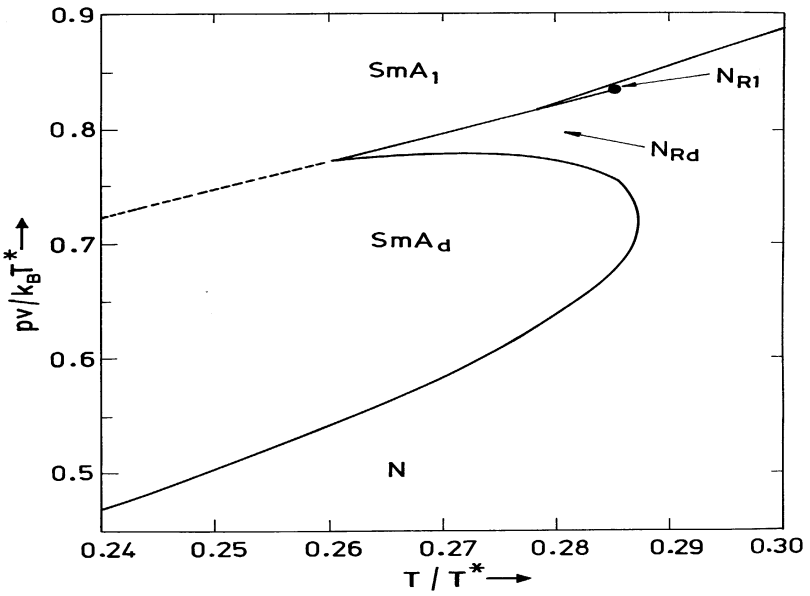

Figure – 5.10. The *p -T* phase diagram obtained for *A* = 1.52, η^* = 0.5, *q* = 1.8 and α_2 = 0.042. The values of (*p, T*) which are indicative of a SmA_1- SmA_d transition are shown by a dashed line. Note the N_{R1} -N_{Rd} transition line ending in a critical point, shown by a filled circle.

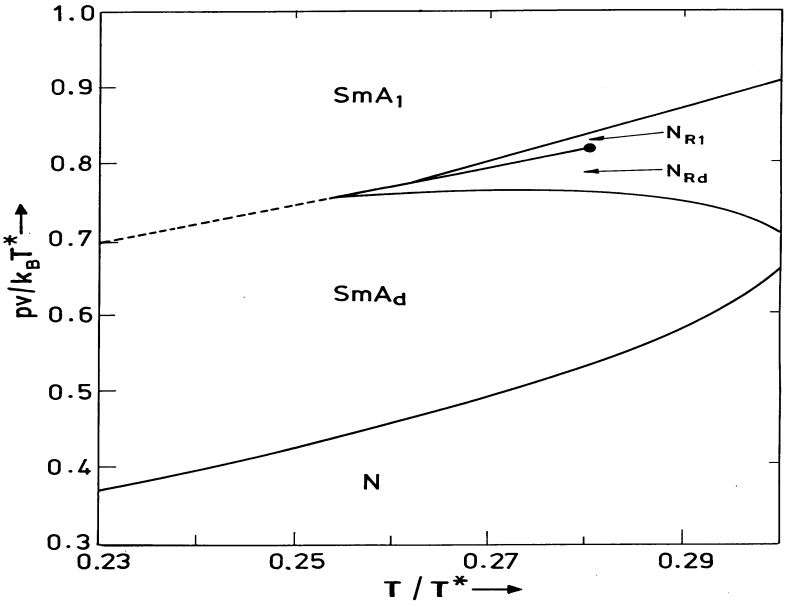

Figure – 5.11. The *p -T* phase diagram obtained for *A* = 1.52, η^* = 0.5, *q* = 1.8 and α_2 = 0.05 and α_1 assumed to be zero. The values of (*p, T*) which are indicative of a SmA_1- SmA_d transition are shown by a dashed line. Note the N_{R1} -N_{Rd} transition line ending in the critical point, shown by a filled circle.

Hence, the packing effect alone is sufficient to stabilise the SmA_1 phase. However, the (p,T) range of the closed SmA_d region has increased as can be expected. The topology of the phase diagram agrees with that predicted using the dislocation loop melting theory of Prost and Toner [27] (see figure 3.6, chapter-3).

As discussed in chapter –3, (section 3.3), when the chain length is increased in a homologous series, ΔE and hence A increase as the fourth power of the McMillan parameter α of the A-type of pairs. In other words, α_2 varies as the fourth root of A. Thus, when A is varied over a small range (0.4 to 1.8), the variation of α_2 is very small. This variation is ignored for simplicity and the effect of variation of A independent of α_2 will be discussed in the next section.

5.3.3 Effect of variation of A independent of α_2

Larger values of the parameter A (see equation 5.1) result in steeper variation of ΔE with respect to the packing fraction η. To study the effect of independent variation of A, we have calculated the phase diagram as a function of pressure and A. We get an N_R lake at the end of a SmA_1 - SmA_d transition line for $\eta^* = 0.5$, $q = 1.8$, T_R=0.28, $\alpha_2 = 0.05$ as shown in the p-A phase diagram (figure 5.12a). This can be understood as follows. When A is small, as the pressure is increased, X_2 has a smoother variation as in the case of pure hard rods (see discussion under section 5.3.2.1) and there is no N_R. For intermediate values of A, ΔE and hence X_2 have a steeper variation with respect to η (and hence p) around $\eta = \eta^*$. Due to packing reasons, when X_2 is decreasing rapidly, the SmA_d phase becomes unstable and the nematic phase reenters. For higher pressures, when X_1 is large, SmA_1 phase becomes stable leading to double reentrance. For larger values of A, X_2 varies quite steeply with respect to η, *i.e.*, upto $\eta = \eta^*$, X_2 is large and for $\eta > \eta^*$, X_1 becomes large. In both cases, SmA phase is stable due to better packing of *similar* molecules. Around $\eta \approx \eta^*$, there is a jump in X_2 (and hence η) which is an indication of SmA_d - SmA_1 transition (shown by dashed line).

As α_2 is *decreased* keeping other parameters fixed, the SmA phase becomes less stable. The N_R lake widens and opens up as shown in figures 5.12(b),(c) and (d)

for α_2 = 0.0475, 0.047 and 0.045 respectively. In figure 5.12b, the N_R lake also has N_{R1} - N_{Rd} transition line changing over to SmA_1- SmA_d transition line. Experimentally Cladis and Brand [28] discovered long ago that the SmA_1-SmA_d transition line ended in a (chiral) nematic lake in a binary mixture containing chiral polar molecules. Experiments on the effect of pressure on such a phase diagram appear not to have been carried out as yet, though the lake has been found in other temperature-concentration phase diagrams [29].

As the lake widens, the SmA_1-SmA_d line continues as N_{R1}-N_{Rd} line which ends in a critical point within the N_R region for lower values of *A* (*i.e.*, effectively for lower homologues). The SmA_1- N_{R1} and the N_{Rd}-SmA_d lines do not meet the N_{R1} -N_{Rd} line at the same point (figure 5.12b), but are separated by the SmA_1- N_{Rd} line. All these results and the topology of the phase diagrams agree with those predicted by the dislocation loop melting theory of Prost and Toner [27] (see figures 3.5 and 3.6, chapter-3).

As mentioned earlier, both *A* and α vary with chain length. Variation of α reflects the variation of chain length in a *homologous series* or that of concentration in a binary mixture of *homologues*. On the other hand, variation of *A* corresponds to the variation of steepness of ΔE with respect to the packing fraction η, not necessarily related to a homologous series. Variation of *A* can also reflect the variation of concentration (*X*) in a binary mixture of chemically *dissimilar molecules*. Hence, the calculated *p-A* diagram can be compared with pressure-concentration (*p-X*) diagrams. Experimentally, phase diagrams in the *p-T* and *T-X* planes only have been reported. Features similar to the those in the theoretical diagrams can be seen in *T-X* diagrams with chemically *dissimilar molecules*. The N_R lake in figure 5.12a and the trends in figure 5.12c are similar to those in the experimental *T-X* diagrams shown in figures 3.4c and 3.22a (chapter-3) respectively. Somasekhara [30] has reported an extensive study of ternary mixtures of (3OBNAB + 4OBNAB) with 9OBCAB where, 3OBNAB is propyloxybenzoyloxy nitroazobenzene, 4OBNAB is butyloxybenzoyloxy nitroazobenzene and 9OBCAB is nonyloxybenzoyloxy cyanoazobenzene. In the experimental temperature- concentration diagrams (figures 6.12 to 6.14 of ref. 29a), it is seen that, the parabolic boundary of the N_R lake points

towards the 'cusp' in the SmA_d - N boundary as in figure 5.12b. Also, as the concentration of the lower homologue 3OBNAB is increased, which is equivalent to decreasing the parameter α in our model, the 'cusp' becomes more pronounced and finally, the N_R lake merges with the main N region (figure 6.15 in ref.29a) as in figure 5.12c.

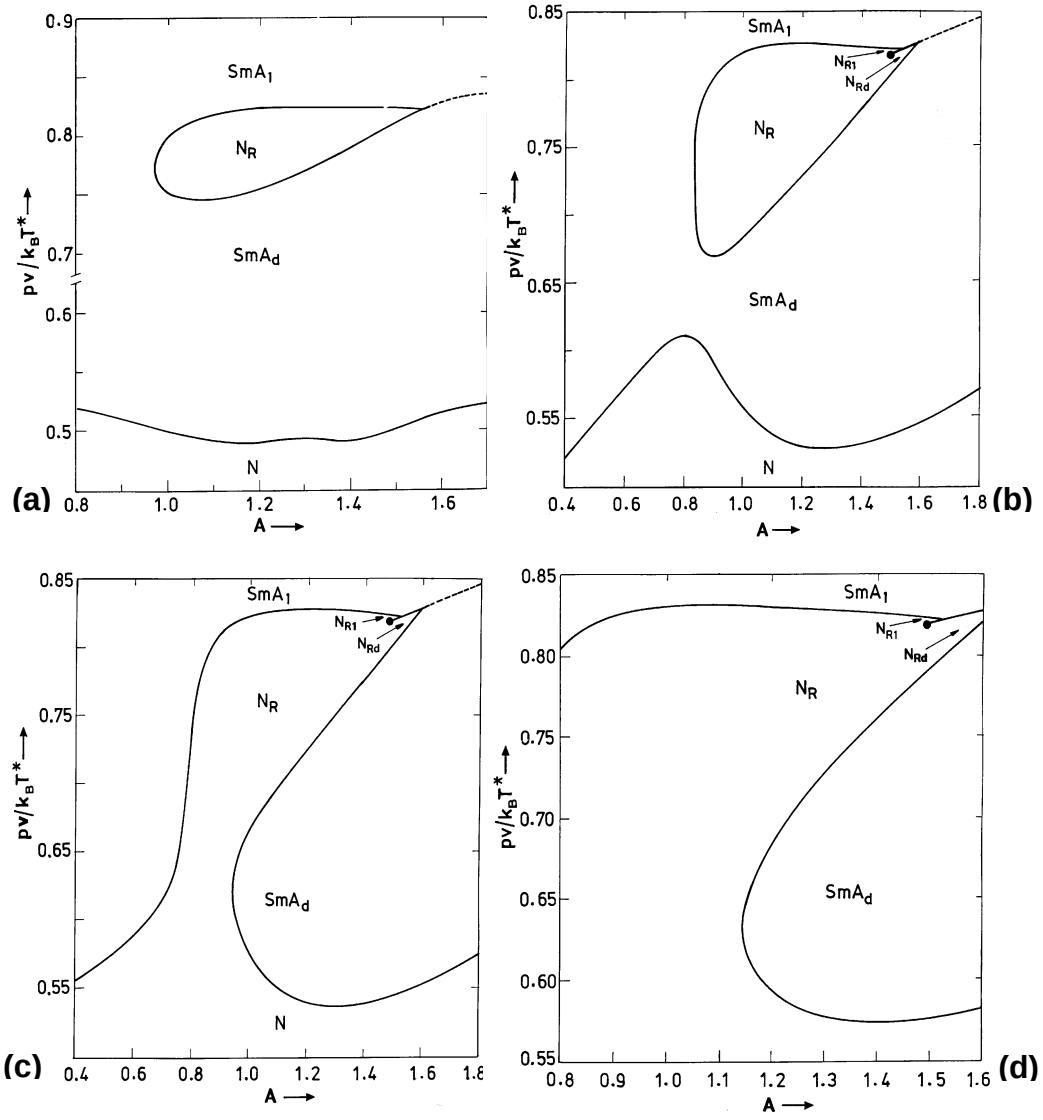

Figure – 5.12. The *p* - *A* phase diagrams with $\eta^* = 0.5$, $q = 1.8$, $T_R = 0.28$ showing the appearance and widening of the reentrant nematic(N_R) lake as the value of α_2 is decreased, (a) the SmA_1-SmA_d transition line ending in N_R lake for α_2 =0.05, (b) wider N_R lake having the N_{R1}-N_{Rd} transition line for α_2 = 0.0475, (c) opening of the reentrant nematic lake creating a 'bay' for α_2 = 0.047 and (d) a wider reentrant nematic bay, for α_2 = 0.045. In the figures, the values of (*p*, *T*) which are indicative of a SmA_1-SmA_d transition are shown by a dashed line and the filled circle indicates the N_{R1} -N_{Rd} critical point.

In principle, as the chain length is varied, *A*, α and *q* vary together. Calculations including all these dependences are somewhat involved and have not been carried out.

Quadruple reentrance is a very rare phenomenon and is seen only in one pure compound [31]. The phenomenon has been predicted by the dislocation loop melting theory [27] and by the spin gas theory [9]. The compound used in reference [31] is DB_9ONO_2 which has the chemical formula $C_9H_{19}O–\phi–OOC–\phi–OOC–\phi–NO_2$ where ϕ denotes the phenyl ring. This compound has a terminal nitro dipole which is oppositely oriented to the two ester dipoles in the core. Hence, antiparallel configurations with different extents of overlappings are possible resulting in smectic polymorphism. This requires a model considering antiparallel configurations with different lengths and configurational energies which is obviously very involved.

However, in our simple model, the possibility of quadruple reentrance at a constant pressure is seen in figure 5.13 which shows the upper part of figure 5.12 (c) in a magnified scale. As *A* is decreased, SmA_d - N_{Rd} - SmA_1 - N_{R1} - SmA_1 transition sequence is obtained as indicated by the dashed line in figure 5.13. It can be noted that the quadruple reentrance occurs only over a very small range of values of the model

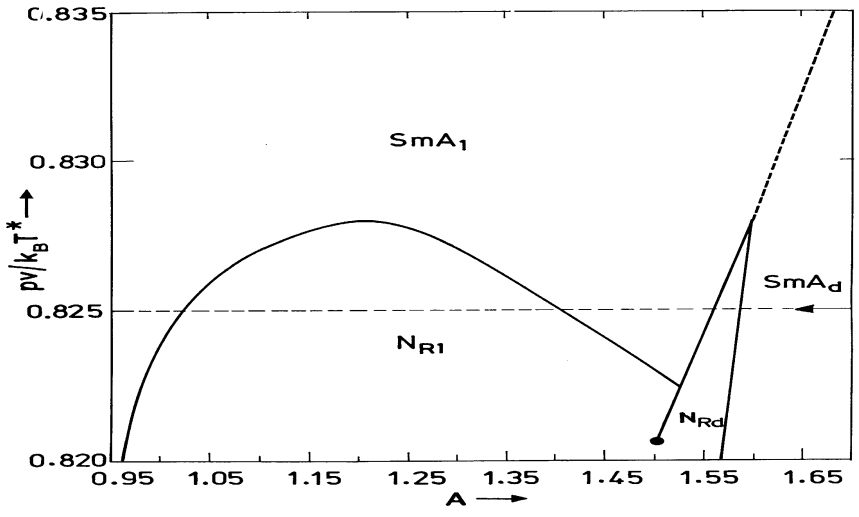

parameters.

Figure – 5.13. The upper part of the figure 5.12c is shown in a magnified scale along the pressure axis. As *A* is decreased, the quadruple reentrant phase sequence SmA_d - N_{Rd} - SmA_1 - N_{R1} - SmA_1 as indicated by the dashed line becomes possible. The filled circle indicates the N_{R1} -N_{Rd} critical point.

In the following section, we consider the effect of independent variations of other parameters of our model.

5.3.4 Effect of variations of other parameters

We consider the effect of independent variations of other parameters of our model to get an idea of the ranges of the parameter values over which the different phases are stable. The effect of variation of α_2 is shown in figure 5.14a for A = 1.5, η^* = 0.5, q = 1.8, T_R = 0.3. For low and high values of α_2, the nematic and the smectic phases respectively are stable over wide ranges of pressures. At intermediate values of α_2, as the pressure is increased, nematic reentrance is seen over a range of pressures corresponding to the steep variation of X_2 due to the change over of the A-type of pairs to P-type of pairs.

The effect of variation of the length ratio (q) of A- and P-types of pairs is shown in figure 5.14b for A = 1.5, η^* = 0.5, α_2 = 0.05, T_R = 0.3. We have varied q up to 1.9 since $q \geq 2$ has no meaning in our model. It can be seen that the nematic reentrance occurs only for intermediate values of q (1.65 to 1.87). For low values of q, A and P types of pairs are structurally very similar. Hence, irrespective of the value of X_2, the SmA phase is stable and there is no nematic reentrance. As the value of q is increased, the structural dissimilarity between the A and P types of pairs increases. Over a range of pressures corresponding to a steep variation of X_2, the layering order is not favoured and the nematic phase reenters. For still larger values of q, the dissimilarity is also large. Thus, the nematic phase is stable over a large range of pressure and the SmA_1 phase appears only at high pressures when the number of P-type of pairs is large. Experimentally, the nematic reentrance is seen when $q \approx 1.4$. In our calculations, a fairly large value of q (≈ 1.65) is required to get the nematic reentrance. This is because the nematic order is assumed to be saturated and the orientational potential is not considered resulting in the increased stability of the

smectic phase. Further, the excluded volume contribution which destabilises the layering order and causes the nematic reentrance, is underestimated due to the second virial approximation.

Note that the trends in figures 5.14 (a) and (b) are opposite though both α_2 and q increase with chain length in a homologous series. As mentioned earlier, an increase of α_2 *alone* increases the stability of the SmA_d phase. On the other hand, an increase of q *independently of* α_2 increases the excluded volume contribution to the free energy and destabilises the SmA_d phase. Experimentally (see for example, figure 3.3a, chapter-3), it is known that in the higher homologues of smectogens the SmA_d phase has greater stability as in figure 5.14a. This indicates that the variation of α_2 is more important in a homologous series than that of q.

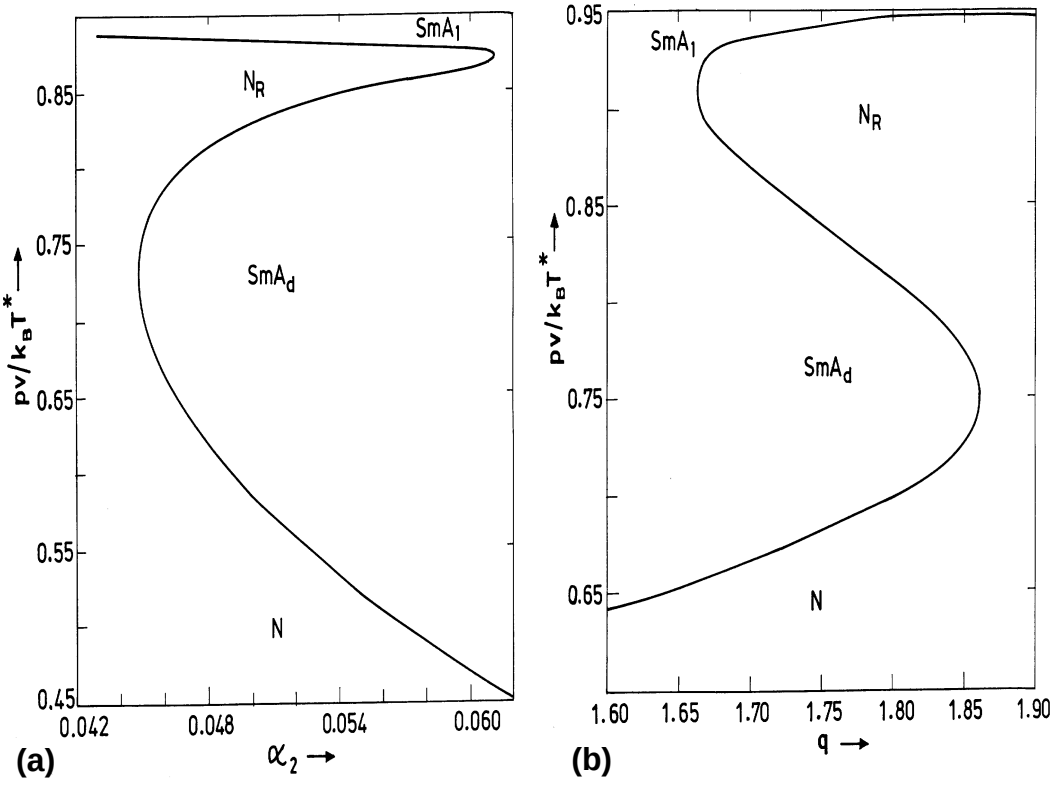

Figure – 5.14. Calculated phase diagrams for A = 1.5, η^* = 0.5, T_R = 0.3 (a) as a function of α_2 with q = 1.8 and (b) as a function of q with α_2=0.05.

In our model, η^* is the packing fraction at which ΔE = 0 (see equation 5.1). Effect of variation of η^* is shown in figure 5.15 for A =1.5, q=1.8, α_2 =0.05, T_R =0.3.

For small values of η^*, X_1 becomes large at relatively low pressures. This results only in the N-SmA_1 transition at high pressures and there is no double reentrance. As the value of η^* is increased, X_2 remains large up to a value of pressure which is sufficient to stabilise the SmA_d phase and results in N-SmA_d transition. At higher pressures, when X_2 starts to decrease, the nematic phase reenters as explained above. For large values of η^*, there is no nematic reentrance since X_1 becomes large only at high pressures. The reentrance of the N phase is associated with the steep variation of X_2 with respect to η which occurs near $\eta \approx \eta^*$. Hence, the range of pressures over which the N_R phase occurs has a strong positive slope with respect to η^*.

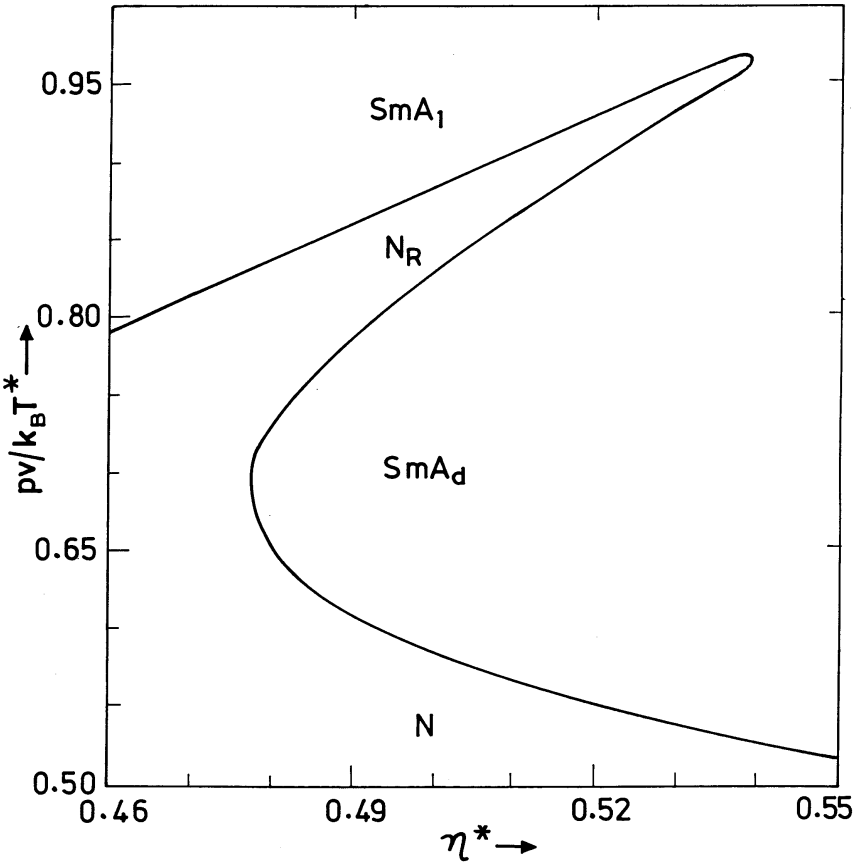

Figure – 5.15. Calculated phase diagram as a function of η^* for A=1.5, T_R = 0.3, q = 1.8 and α_2 = 0.05.

5.4 Conclusions

We have extended our model of highly polar compounds to include the hard core interactions [32], adopting the method used by Koda and Kimura [11]. Assuming perfect orientational order, we have calculated *p-T* phase diagrams showing nematic to

nematic (N_1-N_d) transition, double reentrance with bounded SmA_d region and N_1-N_d transition associated with double reentrance. As the chain length is increased, if the smectic phase does not intervene, the first order nature of the N_1-N_d transition can be expected to become stronger and to occur at a lower temperature at any given pressure. Further, the pressure at which the SmA_d region gets bounded increases with the chain length as seen experimentally. We have also calculated pressure versus *A* phase diagrams, where *A* is a parameter which increases with the chain length in a homologous series. These show the reentrant nematic (N_R) lake associated with the SmA_1-SmA_d transition, N_1-N_d transition occurring inside an N_R lake, quadruple reentrance at constant pressure, and widening and merging of the N_R lake with the main nematic sea. The results are compared with other theories and the available experimental data. Our calculations including the hard core interaction clearly shows that, neglecting the latter is equivalent to a negative deviation in the geometric mean approximation for the attractive mutual interaction between A and P types of pairs and this deviation increases as the two components become structurally more dissimilar.

5.5 References for chapter-5

[1] de Gennes, P. G. and Prost. J., *The Physics of Liquid Crystals* (second edition), Clarendon press, Oxford science publications, 1993.

[2]Madhusudana, N.V., and Jyotsna Rajan, *Liq.Cryst*., **7**, 31, 1990.

[3]Basappa, G., and Madhusudana, N.V., *Eur. Phys. Journal B*, **1**, 179, 1998.

[4]Surjit Dhara and Madhusudana, N.V., to be published.

[5]Cladis, P. E., *Liquid Crystals*, ed Chandrashekhar, S., Heyden Publ, Philadelphia,1980, p105.

[6]Cladis, P. E., Bogardus, R. K., Daniels, W. B., and Taylor, G. N, *Phys. Rev. Lett*, **39**, 720, 1977.

[7] Cladis, P. E., *Mol.Cryst.Liq.Cryst*., **67**, 177, 1981.

[8]Clark, N. A., *J. Phys*, **40**, C3-345, 1979.

[9]Marko, J. F., Indekeu, J. O., and Berker, A. N., *Phys. Rev. A*, **39**, 4201, 1989.

[10]Sear, R., P., and Jackson, G., *Phys. Rev. Lett*, **74**, 4261, 1995.

[11]Koda, T., and Kimura, H., *J. Phys. Soc. Jap.*, **63**, 984, 1994.

[12]Onsager, L., *Ann. N. Y. Acad. Sci.*, **51**, 627, 1949.

[13]Stroobants, A., Lekkerkerker, H. N. W., and Frenkel, D., *Phys. Rev. Lett.,* **57**, 1452; 1986; *Phys. Rev. A,* **36**, 2929, 1987.

[14]Watanabe, J., and Takashina, Y., *Macromolecules*, **24**, 3423, 1991.

[15]Hosino, N., Nakano, H., and Kimura, H., *J. Phys. Soc. Jap.,* **47**, 740, 1979.

[16]Mulder, B., *Phys. Rev. A,* **35**, 3095, 1987.

[17]Wen, X., and Meyer, .R. B., *Phys. Rev. Lett.*, **59**, 1325, 1987.

[18]Taylor, M. P., Hentschke, R., and Herzfeld, J., *Phys. Rev. Lett.,* **62**, 800, 1989.

[19]Poniewierski, A., and Holyst, R., *Phys. Rev. Lett.,* **61**, 2461,1988.

[20]Kimura, H., and Tsuchiya, M., *J. Phys. Soc. Jap.*, **59**, 3563, 1990.

[21]Nakagawa, M., and Akahane, .T, *J. Phys. Soc. Jap.*, **54**, 69, 1985.

[22]Sobha. R. Warrier, Vijayaraghavan, D., and Madhusudana, N.V., *Eur. Phys. Lett*, **44**(3), 296, 1998.

[23]Manjuladevi, V., and Madhusudana, N.V., (to be published).

[24]Mulder, B.M., and Frenkel, D., *Mol. Phy.,* **55**,1193, 1985

[25]Humphries, R. L., James, P. G., and Luckhurst, G. R., *Symp. Faraday Soc.*, **5**, 107, 1971.

[26]Nakagawa, M., and Akahane, .T, *J. Phys. Soc. Jap.*, **52**, 399, 1983.

[27]Barois, P., Prost, J., and Lubensky, T.C., *J.Phys*., **46**, 391, 1985., Prost, J., and Toner., J., *Phys.Rev.A*, **36**, 5008, 1987.

[28]Cladis, P.E., and Brand, H.R., *Phys. Rev. Lett*, **52**, 2261, 1984.

[29]Lie Wu, Garland,C.W., and Pfeiffer, S., *Phy. Rev. A.*,**46**, 973, 1992.

[30]Somasekhara, S., chapter-6 of the Ph.D Thesis "experimental studies of phase transitions in liquid crystals", 1988, *Raman Research Institute*, Bangalore.

[31]Shashidhar, R., Ratna, B. R., Surendranath, V., Raja, V. N., Krishna Prasad, S. and Nagabhushan, C., *J.phys.lett.*, **46**, L-445, 1985.

[32]Govind, A. S., and Madhusudana, N. V., *Liq. Cryst*., **27**, 1249, 2000.